Arabian Journal of Chemistry (2017) xxx, xxx–xxx

King Saud University

Arabian Journal of Chemistry

www.ksu.edu.sa
www.sciencedirect.com

ORIGINAL ARTICLE

# Electrocatalytic activity of starch/$Fe_3O_4$/zeolite bionanocomposite for oxygen reduction reaction

**Nurul Hidayah Abdullah [a], Kamyar Shameli [a,*], Pooria Moozarm Nia [b], Mohammad Etesami [c], Ezzat Chan Abdullah [a], Luqman Chuah Abdullah [d]**

[a] *Department of Environmental Engineering and Green Technology (EGT), Malaysia-Japan International Institute of Technology (MJIIT), Universiti Teknologi Malaysia (UTM), Jalan Sultan Yahya Petra, 54100 Kuala Lumpur, Malaysia*
[b] *Centre of Hydrogen Energy (CHE), Institute of Future Energy, Universiti Teknologi Malaysia, Jalan Sultan Yahya Petra, 54100 Kuala Lumpur, Malaysia*
[c] *Department of Macromolecular Science and Engineering, Case Western Reserve University, 10900 Euclid Avenue, Cleveland, OH 44106, USA*
[d] *Department of Chemical and Environmental Engineering, Faculty of Engineering, Universiti Putra Malaysia, 43400 Serdang Selangor, Malaysia*

Received 20 June 2017; accepted 31 October 2017

**KEYWORDS**

Green synthesis;
Bionanocomposite;
Electrocatalytic;
Oxygen reduction reaction

**Abstract** The present work demonstrated an eco-friendly and facile method for the preparation of starch/$Fe_3O_4$/zeolite-bionanocomposite (BNC) at moderate temperature. Zeolite and starch were used as solid support and stabilizer, respectively. The analysis of UV–vis showed the appearance of surface plasmon resonance. From PXRD analysis, the incorporation of magnetite nanoparticles (NPs) in zeolite substrate results in reducing of intensities and broadening of the zeolite peaks of BNC. The TEM analysis showed the formation of highly distributed $Fe_3O_4$-NPs with an average diameter and standard deviation of 9.24 ± 3.57 nm. The FESEM and EDX analyses imply that $Fe_3O_4$-NPs were homogeneously formed on the surface of the zeolite substrate. VSM analysis illustrated the as prepared BNC possessed magnetic behaviour with a saturation magnetization and coercivity of 1.84 emu $g^{-1}$ and 17.76 G, respectively. The prepared BNC showed potential applicability in energy as low-cost electrode material. The BNC was used as a non-precious catalyst for oxygen reduction reaction (ORR) in the alkaline medium. The presence of starch and zeolite promoted long term stability up to 1000 cycles and avoid the dissolution and agglomeration of iron oxide. The ORR commences at the onset potential of 0 V follows by the two successive reduction peaks at −0.48 V and −1.00 V.



* Corresponding author.
E-mail address: kamyarshameli@gmail.com (K. Shameli).

Peer review under responsibility of King Saud University.

Production and hosting by Elsevier

https://doi.org/10.1016/j.arabjc.2017.10.014
1878-5352 © 2017 Production and hosting by Elsevier B.V. on behalf of King Saud University.
This is an open access article under the CC BY-NC-ND license (http://creativecommons.org/licenses/by-nc-nd/4.0/).

Please cite this article in press as: Abdullah, N.H. et al., Electrocatalytic activity of starch/$Fe_3O_4$/zeolite bionanocomposite for oxygen reduction reaction. Arabian Journal of Chemistry (2017), https://doi.org/10.1016/j.arabjc.2017.10.014

## 1. Introduction

In recent years, there is growing interest in developing environmentally-friendly products based on bionanocomposites. Bionanocomposites (BNCs) are a novel class of nanostructured hybrid materials derived from the combination of natural polymers and inorganic solids with at least one dimension sized in the range of 1–100 nm (Darder et al., 2007; Shchipunov, 2012). Extensive research has been conducted using zeolite-based materials to produce BNCs relative to their unique properties and variability in the frameworks composition. Zeolites are well known microporous crystalline materials with high surface areas and porosity (Chen et al., 2016). Zeolites are safe to be used because they are non-toxic and do not contribute toward eutrophication which is important to preserve biodiversity and promote sustainable ecosystem (Marija Grancaric et al., 2009; Udhoji et al., 2005). Zeolites with framework structure have been investigated as alternative cathode electrocatalyst as they possessed interesting features such as porous structure, high electrical conductivity, thermally stable and promising catalytic activity (Park et al., 2016). The electrical conductivity of variety of zeolites have been reported to be in the range of about $10^{-8}$–$10^{-3}$ $\Omega^{-1}$ $cm^{-1}$ depending on Si/Al ratio and temperature (Freeman and Stamires, 1961; Kelemen and Schon, 1992). Musyoka et al. also demonstrated the thermal stability of zeolite A and X up to 800 °C with the stable crystal structure up to 440 °C (Musyoka et al., 2015).

Among natural polymers, starch is one of the cheap and easily available biomass resources with good biocompatibility and biodegradability characteristics and have granular sizes from submicron to more than 100 μm in diameter (Ahmad et al., 2010; Jane, 2006). Numerous research studies have been reported on the synthesis of starch based BNCs by filling a thermoplastic starch matrix with nanofillers such as montmorillonite (Koriche et al., 2014), bentonite (Koriche et al., 2014), carbon nanotube (Gautam et al., 2015), zeolites (Belibi et al., 2013), and beidellite (Belibi et al., 2013). The development of BNCs with excellent biocompatible and biodegradable properties can be used to replace the non-biodegradable synthetic materials for ensuring the environmental safety and sustainability (Shchipunov, 2012). Besides, the addition of starch may reduce agglomeration among the smaller particles, as it contains many O-H functional groups and can bind to the surface of the nanoparticles at the initial nucleation stage (Ma et al., 2016).

Magnetite ($Fe_3O_4$) is the most studied magnetic iron oxide with an inverse spinel structure and possessed superparamagnetic features in addition to their low toxicity and biocompatibility (Chen et al., 2012; Lu et al., 2010). There are various chemical and physical methods have been introduced for the synthesis of iron oxide nanomaterials such as co-precipitation (Hariani et al., 2013), hydrothermal (Kolen'ko et al., 2014), ultrasonic irradiation (L. Wang et al., 2013a), and thermal decomposition technique (Chin et al., 2011). So far, co-precipitation has been widely employed due to its simplicity, effectiveness, and inexpensive method for the production of iron oxides (Kalantari et al., 2013). The synthesis of iron oxide BNCs have been widely investigated for potential applications in biomedical devices and implants (Das et al., 2013), catalytic reduction of nitroaromatic compounds (Tuo et al., 2015), drug delivery systems (Bukowska et al., 2017) and catalyst support in fuel cell (Gnana kumar et al., 2016; R. Wang et al., 2013b).

Oxygen reduction reaction (ORR) has been credited as one of the promising alternatives for generation of clean energy as it is associated with the process that comprised of the breaking and conversion of chemical energy accumulated in double bonds of oxygen molecules for subsequent production of electrical energy (Mathur et al., 2016). The development of new non-precious cathode catalysts in ORR process for fuel cell and metal-air battery applications is one of the effective strategies to fulfil the highly demands in renewable-energy technologies and storage resources as well as minimizing the dependency towards fossil fuels and petroleum products which are currently running down (Gray, 2009; Jiang et al., 2016; Lin et al., 2014; Mathur et al., 2016; Sun et al., 2015b).

There have been many researchers reported about the use of Pt and its alloys as highly efficient ORR catalysts. However, Pt is known to be expensive and often suffer from decreasing in the activity attributed to the poisoning during the electrooxidation process. Thus, the alternative catalysts based on non-precious metals and metal-free materials have been explored to develop highly durable, stable and cost-effective material with superior activity to replace the scarce Pt (Liang et al., 2011; Sun et al., 2015b). For instance, Tan et al. highlighted the importance of manganese oxides as a template for carbon coating and synergetic active sites for high ORR activity in alkaline solution. The high surface area and stability of the MnO-containing mesoporous nitrogen-doped carbon (m-N-C) nanocomposite also make a significant contribution to high ORR activity and potential cathode catalyst candidate for alkaline methanol fuel cell applications (Tan et al., 2012). Liu et al. have reported the controllable integration of metal-organic frameworks (MOFs) and carbon-based materials by implementing the unique features of ultra-high porosity, synthetic tailorability, facile synthesis and enhanced stabilities and electrical conductivity (Liu et al., 2016). Nitrogen-doped mesoporous carbons and Au nanowires also have been investigated as efficient oxygen reduction catalysts in acidic and alkaline solutions owing to its high electrocatalytic activity (Chu et al., 2013). In addition, three-dimensional sulfur-doped graphene networks have been reported to show high electrocatalytic activity, good stability and excellent methanol tolerance for four-electron oxygen reduction in alkaline solution (Zhang et al., 2014).

The concurrent development of metal oxide based material consisted of $Fe_2O_3$, $Fe_3O_4$, $Co_3O_4$, $MnO_2$, $TiO_2$ and ZnO as non-precious catalyst for ORR process offers incredible advantages for new electrodes engineering and processing (Delmondo et al., 2016; Huijuan Yang et al., 2014; Sun et al., 2015a, 2016, 2017). The significant increase in the surface area of metal oxide material as electrocatalyst may enhanced its catalytic performance by increasing the numbers of catalytic sites that exposed to oxygen (Delmondo et al., 2016). Sun et al. have reported the incorporation of several transition metal oxides with high alkaline corrosion resistance and porosity on graphene substrate to generate an advance ORR electrocatalyst for energy conversion and storage (Sun et al., 2015a). The development of iron oxide based materials as electrocatalyst are significant as they are non-noble catalyst with outstanding catalytic ability, low cost, abundance storage and better durability (Sun et al., 2015a).

Please cite this article in press as: Abdullah, N.H. et al., Electrocatalytic activity of starch/$Fe_3O_4$/zeolite bionanocomposite for oxygen reduction reaction. Arabian Journal of Chemistry (2017), https://doi.org/10.1016/j.arabjc.2017.10.014

Iron oxide/polymer based nanocomposites also have been deposited on solid substrates such as graphene (Gnana kumar et al., 2016), nitrogen doped carbon (CNx) (R. Wang et al., 2013b) and graphene oxide (D. Wang et al., 2017a) to prevent the dissolution and agglomeration of NPs which could result in poor electrocatalytic activity. The soluble starch has been used to produce more stable Pt-NPs in a colloidal state and ensured high monodispersity and formation of small diameter of Pt-NPs. The soluble starch/Pt-NPs deposited on carbon layer demonstrated excellent high stabilities of both electrochemical surface area and ORR compared to the commercialize Pt/C (Cheng et al., 2015). In addition, the encapsulation of metal oxide NPs by soluble starch could improve the stability of metal oxide NPs in water and prevent further aggregation (Ma et al., 2009).

Therefore, in respect to the above-mentioned findings, a new type of non-precious and low cost electrocatalyst based on starch/$Fe_3O_4$/zeolite-BNC was developed to study its electrocatalytic activity for ORR process. The preparation of BNC based on green synthesis technique was implemented by controlling three main aspects such as solvent, reducing agent and stabilizing agent that significance to eliminate the use or generation of hazardous substances. The used of soluble starch and zeolite may improve the stability of the prepared BNC for oxygen reduction reaction and provide high surface area and porosity for efficient ORR activity. Therefore, the unique properties of starch and zeolite as stabilizer and solid support were further explored for the preparation of iron oxide-NPs to develop novel eco-friendly BNC material for potential energy application.

## 2. Experimental

### 2.1. Materials and apparatus

All chemicals and reagents were of analytical grade and used as received without further purification. Ferric chloride hexahydrate ($FeCl_3$ś$6H_2O$, 97%), ferrous chloride tetrahydrate ($FeCl_2$ś $4H_2O \geq 96\%$) and zeolite 3A powder (0.6 $K_2O$: 4.0 $Na_2O$: 1 $Al_2O_3$: 2.0 ± 0.1 $SiO_2$: x $H_2O$) were acquired from Sigma Aldrich. Sodium hydroxide (NaOH, 99%) and soluble potato starch $(C_6H_{10}O_5)_n$ were supplied by R&M Chemicals. Deionized water from ELGA Lab Water Purification System, UK was used as medium for the synthesis of material. The benchtop pH meter model sensION + MM374 GLP 2 was employed to control the solution pH. The prepared samples were dried in an Esco Isotherm Forced Convection Laboratory Oven.

### 2.2. Preparation of starch/$Fe_3O_4$/zeolite bionanocomposite

The experiment was conducted according to the method described by Abdullah et al. (2017b) with a slight modification. First, 2.0 g of zeolite was suspended in 50 mL of deionized water. Subsequently, NaOH (0.5 M) was added to the zeolite suspension (pH ~ 12.8) and continue stirred for 20 min. Then, a mixture of $Fe^{3+}$ (0.228 M) and $Fe^{2+}$ (0.114 M) solution with 2:1 ratio and pH of ~1.4 was added into 0.3 g hot starch solution (0.006 g $ml^{-1}$) at 60 °C. Next, the resulting mixture was added dropwise into the zeolite suspension. A subsequent amount of NaOH (0.5 M) was added to maintain the solution pH to 11. The stirring was continued at moderate temperature around 40 °C for 30 min. The precipitates were centrifuged at 10,000 rpm, washed several times with deionized water, and finally dried in an oven at 50 °C for 24 h.

### 2.3. Characterization of starch/$Fe_3O_4$/zeolite bionanocomposite

Various instrumentation techniques, such as ultra-violet visible spectroscopy (UV–vis), powder X-ray diffraction (PXRD), transmission electron microscopy (TEM), Field Emission Electron Microscopy (FESEM) equipped with Energy Dispersive X-ray (EDX), vibrating sample magnetometer (VSM) and Fourier transform infrared spectroscopy (FT-IR) were adopted to characterize the prepared starch/$Fe_3O_4$/zeolite-BNC. The UV–visible spectral measurements were carried out using UV–Vis spectrophotometer (UV-1800, Shimadzu) over the range of 300–800 $cm^{-1}$ by simply adding a colloidal dispersion (in distilled water) into a cuvette, and gently shaken before the reading was taken. The crystallinity and phase purity of the samples were examined by PAN analytical X'pert PRO at an applied current of 20 mA and accelerating voltage of 45 kV with Cu Kα radiation (λ = 1.54 Å) at 2θ angle configuration scanning from 5° to 80° (scanning rate = 2°/min). The size and morphology of the samples were observed under TEM model Tecnai™ $G^2$ F20 series. A drop of dispersed nanoparticles was dripped onto 300-mesh copper grids and air dried before viewing under a microscope. The microscope was operated at accelerating voltage from 20–200 kV and standard magnification from 22 X to 930 KX. The morphology of the samples was observed by FESEM-JEOL JSM-7600 F equipped with EDX (Oxford Instrument spectrometer) with accelerating voltage from 5–15 kV and magnification from 5 KX to 100 KX. The preparation of the samples can be done by attaching a thin layer of powder sample on the carbon tape and coating with the platinum to reduce charging effect. The VSM analysis was carried out at room temperature to determine the magnetic properties of the BNC. The FT-IR spectra were measured over the range of 400–4000 $cm^{-1}$ using the Nicolet 6700 FT-IR spectrometer to determine the presence of functional groups associated with the compounds. The samples were prepared by grounding the dried samples with potassium bromide (KBr) to produce pellet before being analyzed.

### 2.4. Electrochemical test

Versa STAT3 employing Versa Studio software was used to perform the linear sweep voltammetry (LSV) and cyclic voltammetry for the electrochemical characterization. The tests were conducted using a conventional three-electrode electrochemical cell. The modified glassy carbon electrode (BNC/GCE), a Pt wire and a Ag/AgCl electrode were used as the working, auxiliary and reference electrodes, respectively. The preparation of BNC/GCE was performed by sonication of 1 mg/mL of BNC for 30 min and 30 μL of the dispersed sample was dropped on GCE (surface area: 0.07068 $cm^2$). The electrocatalytic activity of the BNC was evaluated to study its potential as electrocatalyst for the oxygen reduction reaction (ORR). The ORR was investigated by LSV and CV techniques in an $O_2$-saturated 0.1 M KOH solution. The nitrogen and oxygen gasses were purged into the KOH solution for 30 min before running the electrochemical tests. The electrochemical stability

test was conducted using CV analysis up to 1000 cycles in an $O_2$-saturated 0.1 M KOH solution.

## 3. Results and discussion

### 3.1. Synthesis of starch/$Fe_3O_4$/zeolite bionanocomposite

Fig. 1 shows the formation of white cloudy zeolite suspension in NaOH (0.5 M) solution. The zeolite suspension gradually changed to dark brown precipitates with the addition of an aqueous mixture of $Fe^{3+}$ and $Fe^{2+}$ ions in hot starch solution and subsequent addition of NaOH solution. The synthesis of $Fe_3O_4$/starch complex on the zeolite substrate involved the interaction between external surface of $Fe_3O_4$ nanoparticles with positive charge and oxygen atoms in hydroxyl group of starches as negative charge (Dung et al., 2009; Zhang et al., 2011). The chemical bonding between soluble starch and zeolite structure also can be observed indicated the starch was adsorbed onto the zeolite surface (Yan et al., 2014). Moreover, previous studies reported that starch can form complexes with metal ions because of their high number of coordinating functional groups (hydroxyl and glucoside groups) and act as templates for nucleation and initial crystal growth of iron oxide (Chang et al., 2011; Ma et al., 2009; Yu et al., 2009). Furthermore, the presence of polysaccharides compound may generate dynamic supramolecular associations through inter- and intramolecular hydrogen bonding, as well as hindering agglomeration of the particles, and producing nanoparticles of smaller sizes. The existence of starch may improve the dispersion of iron oxide NPs on the zeolite surface and in the aqueous solution. The formation of magnetic BNC can be confirmed upon attraction of the material towards external permanent magnet (Fig. 1).

In this study, a small amount of starch (0.3 g) was used to assure better dispersion of iron oxide nanoparticles and prevent the excess starch from capping iron oxide NPs (Chang et al., 2011; Mao et al., 2016). Mao et al. reported that too much starch in the composite material would result to decrease in the catalytic performance (Mao et al., 2016). Chang et al. demonstrated a small amount of soluble starch (14.3 wt%) was utilized for the formation of uniform iron oxide NPs on the surface of the multiwall carbon nanotube (MWCNT) composites (Chang et al., 2011). On the other hand, Wang et al. discovered that the optimum mass ratio of 12:5 of iron oxide to starch would give high saturation magnetization and high specific surface area (S. Wang et al., 2017b). In addition, Zhang et al. presented that the increased in starch loading from 0 to 0.5 wt% resulted to decrease in the NPs sizes from 124.7 nm to 11.5 nm. At elevated starch concentration, the surface of each particle was slowly covered with stabilized molecules, which induce a strong steric repulsion force thus hindering the aggregation of particles and allow complete stabilization of the particles (Zhang et al., 2011).

Eq. (1) displayed the metal ions were compounded with starch and complex ions were generated [starch/$2Fe^{3+}$:$1Fe^{2+}$]. In the Eq. (2), sodium hydroxide was added to reduce the ions in [Zeolite/starch/$2Fe^{3+}$:$1Fe^{2+}$] to [Zeolite/starch/$Fe_3O_4$] precipitates. The overall reaction for the formation of zeolite/starch/$Fe_3O_4$-BNC may be written as follows:

$$\text{starch} + H_2O_{(l)} + 2Fe^{3+}_{(aq)} + Fe^{2+}_{(aq)} \xrightarrow{\text{Stirring}} [\text{starch}/2Fe^{3+} : 1Fe^{2+}] \quad (1)$$

$$[\text{Zeolite/starch}/2Fe^{3+} : 1Fe^{2+}] + 8OH^-_{(aq)} \xrightarrow{\text{Stirring}} [\text{Zeolite/starch/}Fe_3O_4]_{(s)} \downarrow + 4H_2O_{(l)} \quad (2)$$

### 3.2. UV–visible analysis

The UV–Vis spectroscopy of starch, zeolite, $Fe_3O_4$ and starch/$Fe_3O_4$/zeolite-BNC are illustrated in Fig. 2. From the spectra, starch (yellow) and zeolite (blue) do not show any absorption peak. On the other hand, the samples consisted of $Fe_3O_4$-NPs showed the appearance of surface plasmon resonance absorption peak (Fig. 2(c) and (d)). The spectrum of $Fe_3O_4$ and BNC showed that the absorption intensity decreased with the increased of the wavelength in the range of 300–800 nm and no strong absorption peak was identified in this region. Hui et al. reported the similar occurrence was observed with no obvious peak attributed to the $Fe_3O_4$-NPs formation in the UV–vis spectrum (Hui et al., 2011). A broad featureless peak corresponded to the core–shell structure of the NPs can be seen

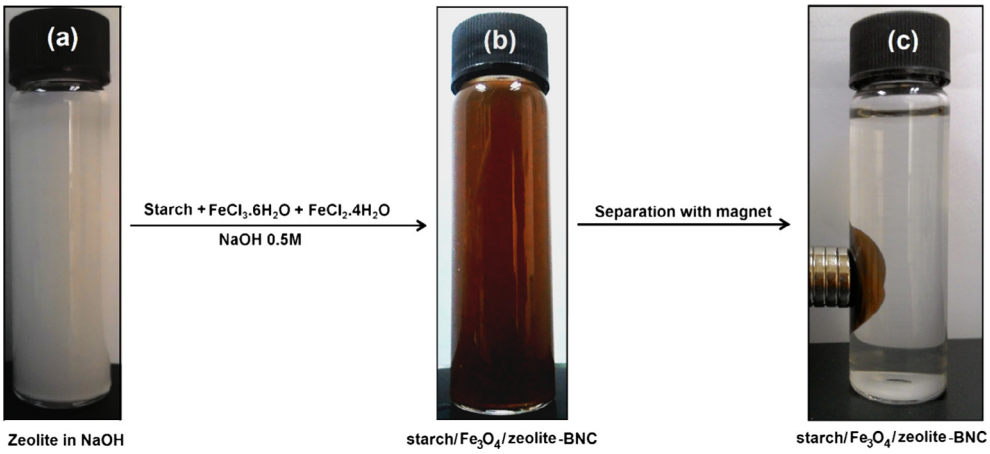


**Fig. 1** Zeolite suspension (a), starch/$Fe_3O_4$/zeolite-BNC (b), separation of BNC from reaction mixture using an external magnet (c).

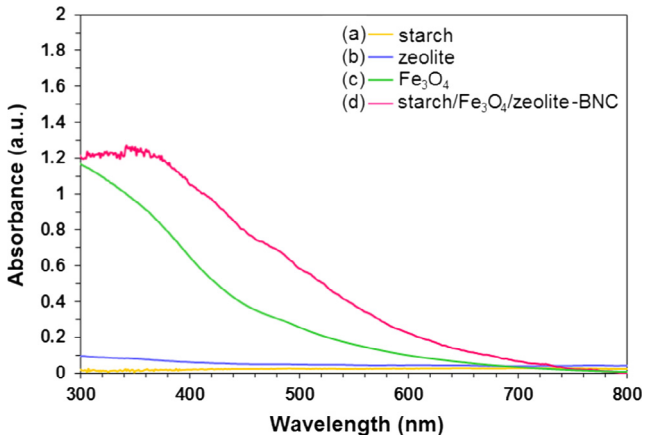


**Fig. 2** UV–visible spectra of (a) starch (b) zeolite (c) starch/$Fe_3O_4$/zeolite-BNC.

at a wavelength of about 380 nm in the spectrum of $Fe_3O_4$@$SiO_2$ NPs due to the changes of band gap caused by the quantum size effect and surface effect of the nanostructures (Hui et al., 2011). In case of starch/$Fe_3O_4$/zeolite-BNC, the intensity of the absorption peaks was increased owing to mixed transition of composite.

### 3.3. Powder X-ray diffraction

The PXRD patterns of zeolite (Abdullah et al., 2017b), zeolite treated NaOH (Abdullah et al., 2017b), starch/$Fe_3O_4$/zeolite-BNC and potato starch (Abdullah et al., 2017a) are shown in Fig.3 (a-e). The PXRD pattern of starch/$Fe_3O_4$/zeolite-BNC (Fig.3c) demonstrated the substantial loss of crystallinity and shifting of the peaks toward higher angle due to the incorporation of starch/$Fe_3O_4$-NPs along with the substantial induce of the mesoporosity (Abdullah et al., 2017a, 2017b). In addition, the introduction of mesopore formation are significant due to the purely microporous feature of zeolites can be a drawback in particular applications as it could inflicts the diffusion limitations which results to a restricted access to the porous structure whenever the bulky molecules are involved (Paixao et al., 2011).

Moreover, decreased in the crystallinity was also associated with the massive dissolution of zeolite particles and loss of both Si and Al atoms (Sadowska et al., 2013). By comparing the PXRD pattern of BNC with our previous reported works (Abdullah et al., 2017a, 2017b), all the peaks were corresponded to the cubic zeolite phase (JCPDS file no: 00-038-0241). Fig. 3e also displayed the overlapping of $Fe_3O_4$ peaks with zeolite phase at 2θ of 30.33°, 36.07°, 43.16°, 53.52°, 56.77° and 63.01°. The incorporation of iron oxide-NPs on zeolite substrate results in broadening of peaks at 2θ = 36.07° and 63.01° which correspond to the most intense of magnetite peaks (JCPDS file no: 019-0629). Nonetheless, no appearance of starch phase was observed in BNC due to the small amount of starch was used during preparation of BNC.

### 3.4. Field emission scanning electron microscopy analysis

In Fig. 4, the surface of cubic zeolite structures becomes rough with the formation of starch stabilized $Fe_3O_4$-NPs. More opening of the zeolite pores can be attributed to the significant induce of mesoporosity after desilication with NaOH and addition of starch (Sadowska et al., 2013; Zhang et al., 2016). Abdullah et al. reported the zeolite exhibited cubic shape morphology with a smooth surface and composed of Al, Si, Na and O elements (Abdullah et al., 2017b). The incorporation of iron oxide-NPs in zeolite was verified by the appearance of Fe element at regions approximately 0.7 and 6.4 keV (Fig. 4(b)). The decrease of Si/Al atomic ratio of zeolite from 1.02 (Abdullah et al., 2017b) to 0.86 was confirmed by EDX analysis of BNC sample. The introduction of soluble starch could reduce the agglomeration of $Fe_3O_4$ on the surface of zeolite substrate. The synthesized BNC may serve as electrocatalyst for effective ORR reaction owing to its high surface area and porosity.

### 3.5. Transmission electron microscopy analysis

TEM images (Fig. 5(a) and (b)) revealed the formation of nanoparticles of irregular shape corresponded to starch-stabilized $Fe_3O_4$-NPs on the zeolite surface. A histogram illustrated that the as-synthesized NPs have an average diameter and standard deviation of 9.24 ± 3.57 nm (Fig. 5(c)). The selected-area electron diffraction (SAED) pattern in Fig. 5(d) showed that the pattern can be assigned to [2 2 0], [3 1 1], [4 0 0], [5 1 1] and [4 4 0] planes of cubic $Fe_3O_4$ which is in agreement with the XRD pattern (JCPDS file No. 019-0629). From these results, highly dispersed NPs with small diameter sizes have been synthesized and could be further used as electrocatalyst for ORR process. The small particle sizes with less agglomeration may provide high surface area of catalyst for effective electrocatalytic activity.

### 3.6. Vibrating sample magnetometer analysis

The VSM result of starch/$Fe_3O_4$/zeolite-BNC is shown in Fig. 6. The result showed that the sample exhibited magnetic properties at room temperature with coercivity ($H_c$) and remanance ($M_r$) of 17.76 G and 0.0034 emu/g, respectively. The saturation magnetization ($M_s$) obtained was 1.84 emu/g. Low saturation magnetization was attributed to the presence of non-magnetic layer of the starch and zeolite as well as low iron oxide loading. Low saturation magnetization also has been reported for zeolite/$Fe_3O_4$-NCs as this is common occurrence for the hybrid nanoparticle systems (Murbe et al., 2008; Sagir et al., 2016). They deduced that the difference in spin ordering at the surface of the particles over that in the bulky material resulting a magnetic core–shell structure. Moreover, the weaker magnetization and lack of saturation signified the characteristic of superparamagnetic NPs with grain size smaller than 20 nm (Murbe et al., 2008; Sagir et al., 2016). However, the BNC prepared in this study demonstrated the presence of small coercivity of ~17.76 G attributed to the ferromagnetic behaviour of $Fe_3O_4$. Similar finding also has been reported for $Fe_3O_4$-NPs prepared using leaf extract that demonstrated ferromagnetic behaviour at 300 K with larger coercivity of 230 G although the particles sizes obtained were around 6 nm (Basavegowda et al., 2014). In case of ferromagnetic material although the magnetic field has been removed, there is still a little amount of magnetization remains which is called remnant magnetization as its value can be varied

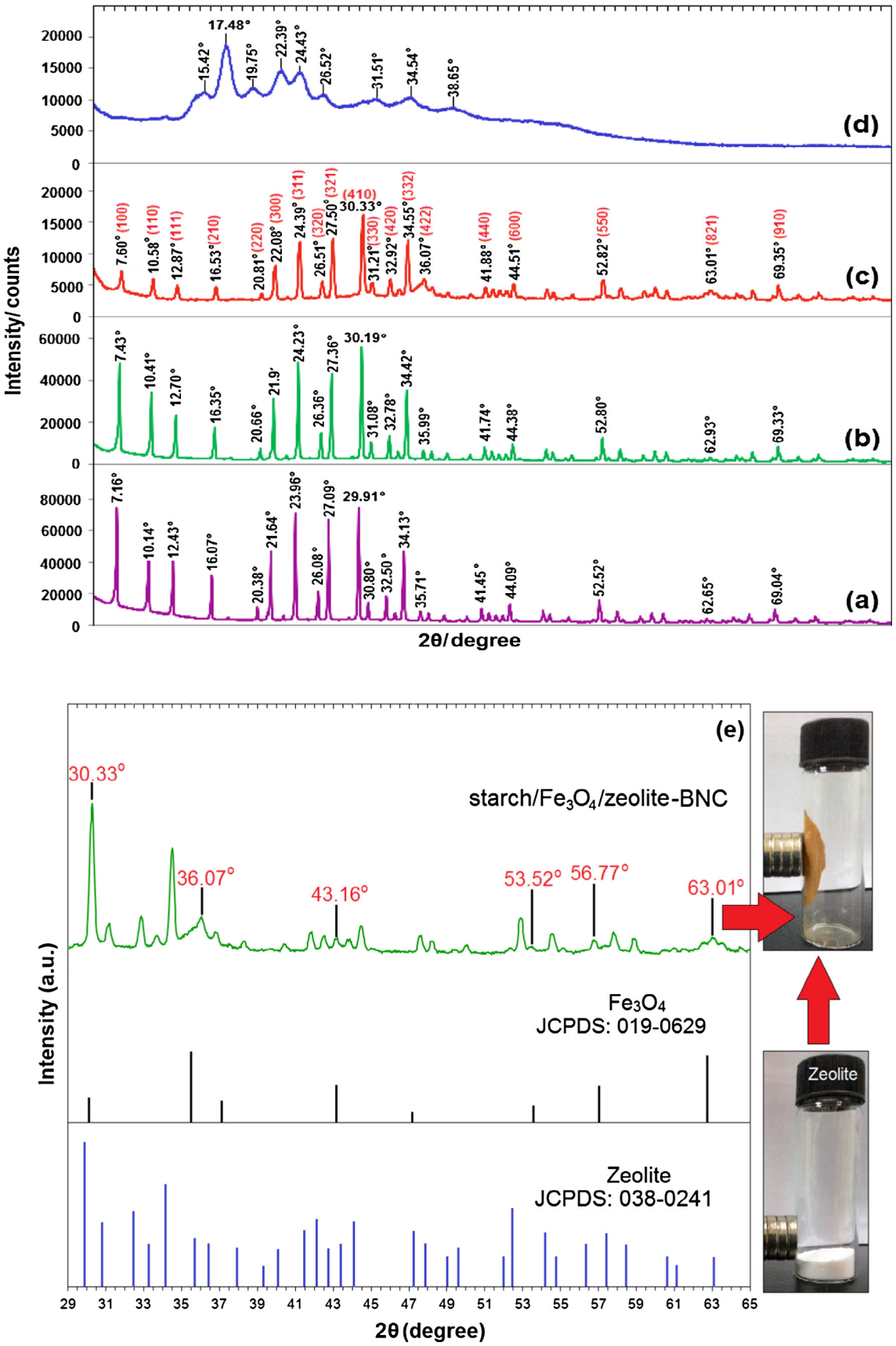


**Fig. 3** PXRD patterns of zeolite (a), zeolite treated NaOH (b) starch/$Fe_3O_4$/zeolite-BNC (c, e), potato starch (d).

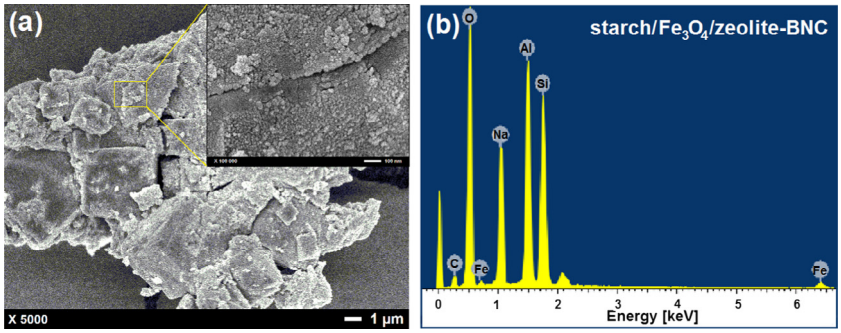


**Fig. 4** FESEM images of starch/$Fe_3O_4$/zeolite-BNC (a) and composition analysis by EDX (b).

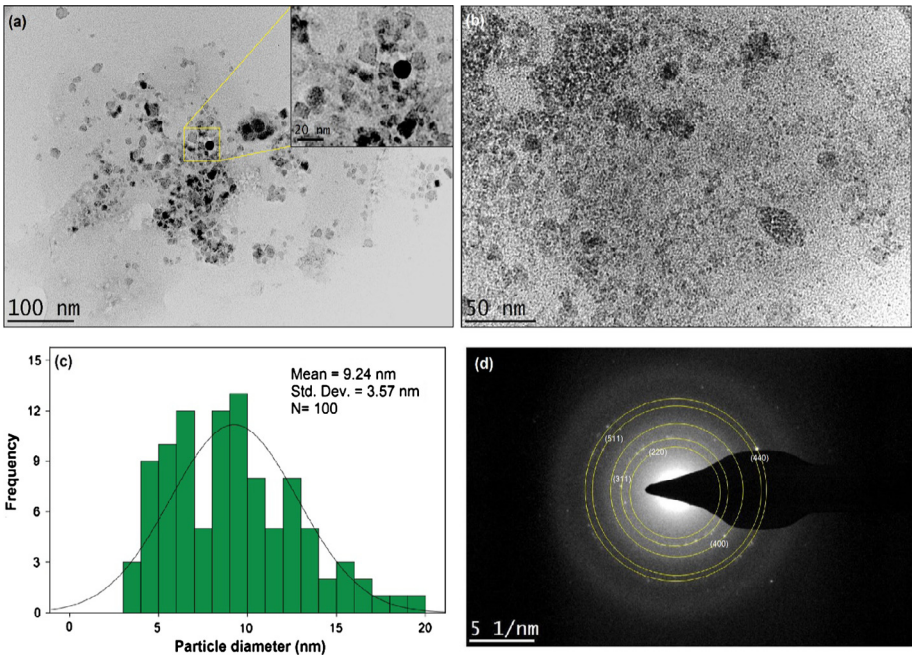


**Fig. 5** TEM images of starch/$Fe_3O_4$/zeolite-BNC (a,b), Particle size distribution of BNC (c) SAED pattern of $Fe_3O_4$-BNC (d).

depending on the structural, microstructural, and compositional parameters of materials (Ghazanfari et al., 2016). Thus, coercive field at the opposite direction is applied to destroy the remnant magnetization (Ghazanfari et al., 2016). In ORR process, the enhancement of the ORR current in ferromagnetic samples has been observed when high external magnetic fields were applied which facilitate the oxygen transfer on the cathode as a result from the existence of strong Kelvin (magnetic) force. Wang et al. demonstrated the synthesis of different types of ferromagnetic catalyst with saturation magnetization (Ms) of 86.3, 68.5, and 0.78 emu $g^{-1}$, for $Fe_3O_4$, $\gamma$-$Fe_2O_3$, and Fe-N-C, respectively (Wang et al., 2016). They reported the increase of the ORR current on Fe-N-C is larger than $Fe_3O_4$ and $\gamma$-$Fe_2O_3$ correspond to some internal tiny magnetic fields produced by the $Fe_3O_4$ and $\gamma$-$Fe_2O_3$ catalysts were different from the magnetic direction of the external magnet. In addition, the ORR current on the cathode also increased as the strength of the external magnetic field increased. However, if the applied external magnetic field is lower than the saturation magnetization of the ferromagnetic catalysts, the existence of internal tiny magnetic field in the ferromagnetic catalysts would lessen the oxygen transfer. Moreover, it was noted that the direction of the external magnetic field does not affect the $O_2$ transfer due to the paramagnetic behaviour of the oxygen moleculars (Wang et al., 2016). Therefore, based on the aforementioned aspect we can deduced that BNC with ferromagnetic behaviour and low saturation magnetization can be further used as electrocatalyst in ORR process.

### 3.7. Fourier transform infrared analysis

Fig. 7 showed the FTIR spectrum of starch/$Fe_3O_4$/zeolite–BNC. The spectrum showed the appearance of strong and broad absorption band in the region of 3424 $cm^{-1}$ attributed to the terminal silanol groups (Si—O-H) on the external surface of the zeolite crystals (Sagir et al., 2016). The featured peak also represent inter and intermolecular hydrogen bonding in the spectral regions of 3000–3600 $cm^{-1}$ (Ahmad et al., 2010; Sagir et al., 2016). The appearance of band in the region of 1653 $cm^{-1}$ was corresponded to O-H bending vibration of

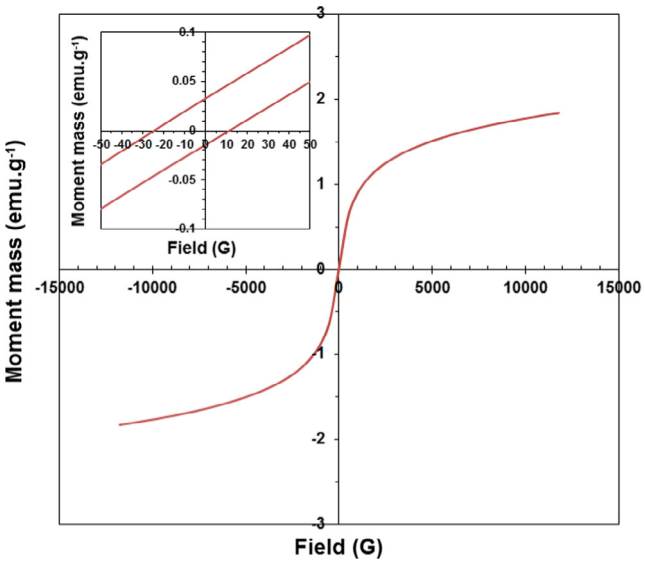


**Fig. 6** Magnetization versus applied magnetic field for starch/$Fe_3O_4$/zeolite–BNC at 300 K. The inset of enlarged hysteresis loop, showing a coercive field.

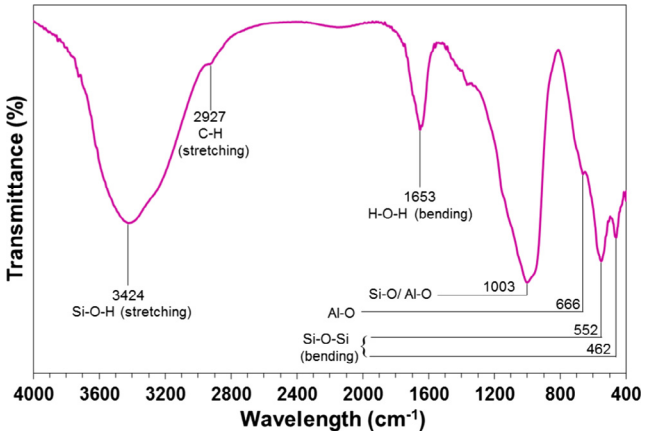


**Fig. 7** The near FT-IR spectra of starch/$Fe_3O_4$/zeolite–BNC.

bound water in starch. The assigned peaks in the region of 900–1200 $cm^{-1}$ were attributed to the stretching and bending modes of Si-O and Al-O in the zeolite framework (Loiola et al., 2012). For instance, the band that appeared around 1003 $cm^{-1}$ was associated with the asymmetric and symmetric stretching modes of external linkages of Si-O and Al-O. The band observed in the region of 666 $cm^{-1}$ was attributed to the Al-O vibration. Meanwhile, the corresponding bands observed at wavelength of 552–462 $cm^{-1}$ were associated with the Si-O-Si bending vibration (Shameli et al., 2011). The appearance of small peak at 2927 $cm^{-1}$ due to the C-H stretching vibration of starch compound indicated the starch was adsorbed onto the zeolite surface (Yan et al., 2014). Apart from that, the incorporation of $Fe_3O_4$ and starch in zeolite structure also results to the peaks broadening at wavelength below 800 $cm^{-1}$. The Fe-O bands attributed to the spinel structure in the range between 400 and 800 $cm^{-1}$ were found to be overlapped with broad Si-O and Al-O band vibration at 462, 552 and 666 $cm^{-1}$ (Murbe et al., 2008). Similar observation also has been reported for magnetite/zeolite NCs with the overlapping of Fe–O band vibration with Si-O at 445 $cm^{-1}$ (Sagir et al., 2016). Moreover, the C-O band attributed to the starch molecule also overlapped with Si-O or Al-O stretching vibration at 1003 $cm^{-1}$. The FTIR analysis of zeolite and potato starch have been reported in the previous works (Abdullah et al., 2017a, 2017b).

### 3.8. Application in oxygen reduction reaction

ORR is an important reaction in electrochemical energy storage/conversion devices. The ORR occurs in half cell of the electrochemical devices such as metal-air batteries and direct methanol fuel cells (DMFCs). The two main proposed ORR pathways, 2-electron (Eq. (3)) and 4-electron pathways (Eq. (4)) in alkaline solution have been shown as follows:

$$O_2 + H_2O + 2e \rightarrow OH^- + HO_2^- \quad \text{(2-electron pathway)} \qquad (3)$$

$$H_2O + HO_2^- + 2e \rightarrow 3OH^-$$

$$O_2 + 2H_2O + 4e \rightarrow 4OH^- \quad \text{(4-electron pathway)} \qquad (4)$$

Fig. 8 displays the comparison between the performance of BNC and $Fe_3O_4$/starch in the $O_2$-saturated and BNC in the $N_2$-saturated 0.1 M KOH solution by LSV. The voltammograms show that the BNC is a good catalyst for reducing oxygen molecules in the presence of $O_2$ saturated whereas no significant ORR activity in $N_2$-saturated 0.1 M KOH solution. The oxygen reduction commences at the onset potential of 0 V follows by the two successive reduction peaks at −0.48 V and −1.00 V. The hydrogen evolution starts at the potential about −1.42 V. The ORR performance of BNC was compared with the previous reported $Fe_3O_4$/zeolite-NC (Abdullah et al., 2017b). The ORR activity between NC and BNC did not showed any significant different. This might be due to the low starch contain was used during preparation of BNC. The starch was added to improve the stability of cathode catalyst as the strong chemical bonding between starch and $Fe_3O_4$ may prevent the iron oxide from undergo dissolution ang aggregation after long term-stability test. However, if the amount of starch was too much it would result to decrease in catalytic activity due to the iron oxide NPs were capped

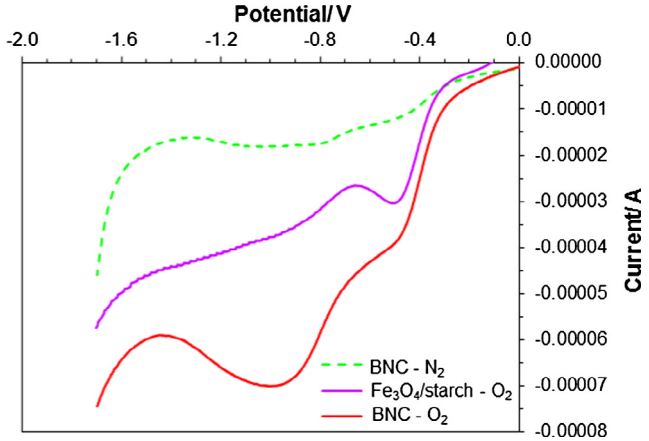


**Fig. 8** Linear sweep voltammograms of BNC in $N_2$, $Fe_3O_4$/starch-$O_2$-saturated, BNC-$O_2$-saturated 0.1 M KOH.

by starch (Mao et al., 2016). The low ORR activity was observed for the sample containing only $Fe_3O_4$/starch (Fig. 8). The ORR activity was found to be lowered than NC and BNC. This occurrence was attributed to the low amount of iron oxide contains as compared to starch (Abdullah et al., 2017a). Thus, to improve the performance of ORR activity of $Fe_3O_4$/starch, a high ratio of $Fe_3O_4$ to starch is required.

Cyclic voltammetry (CV) was employed to investigate the electrochemical activity of the prepared materials toward oxygen reduction reaction. In order to investigate the ORR performance of synthesized materials, CV was carried out in 0.1 M KOH in the of oxygen saturated. Oxygen reduction reaction of bare GCE, starch/$Fe_3O_4$, and starch/$Fe_3O_4$/zeolite-BNC are shown in Fig. 9. For the bare electrode, no ORR activity was recorded under the presence of $O_2$ at the selected potential range from 0 to −1.7 V. Fig. 10 shows that the bare $Fe_3O_4$-NPs exhibits the highest oxygen reduction activity centered at −1.1 V. From Fig. 11, the LSV of bare $Fe_3O_4$-NPs showed significant ORR activity at the onset potential of 0 V follows by the two successive reduction peaks at around −0.40 V and −1.1 V. As can be seen in Fig. 9, other modified electrodes do not show any obvious reduction peak in the selected potential window. Although the ORR of the starch/$Fe_3O_4$ and BNC was smaller than solely $Fe_3O_4$, but based on the literature, $Fe_3O_4$ does not have enough stability for a long time due to easy dissolution, sintering and agglomeration (Huijuan Yang et al., 2014).

The ORR stability of BNC in 0.1 M KOH solution was carried out via CV after cycling for 1000 cycles (Fig. 12). The synthesized material was subjected to 1000 sweep cycles between 0.0 and -1.8 V *vs.* SCE at a scan rate of 50 mV/s. As can be seen from Fig. 13, the current response did not show considerable decrease after 1000 cycles and the material retains around 95% of its initial response ($I_0$ and $I_t$ are the response current in the first and following days, respectively). It confirms that the synthesized material shows high stability for ORR in alkaline solution. The incorporation of starch as stabilizer, results to well maintained of the ORR activity as the stability increased which mainly due to synergetic effect between $Fe_3O_4$ and starch.

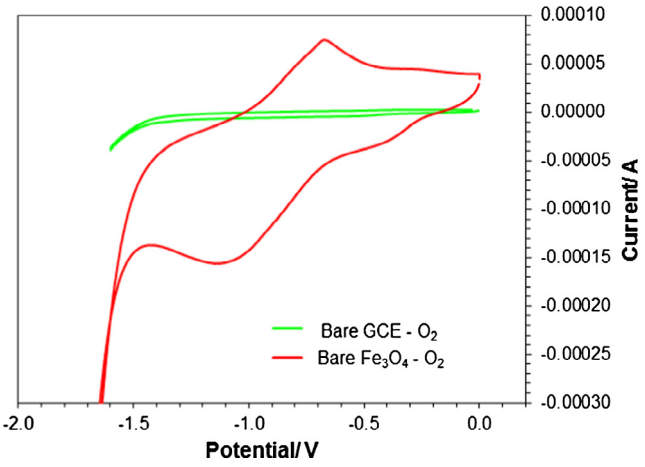


**Fig. 10** Cyclic voltammetry for bare GCE and bare $Fe_3O_4$ in $O_2$-saturated 0.1 M KOH.

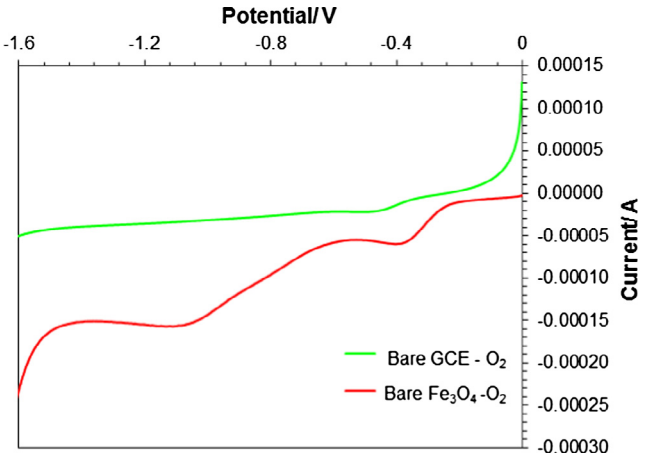


**Fig. 11** Linear sweep voltammograms of bare GCE and bare $Fe_3O_4$ in $O_2$-saturated 0.1 M KOH.

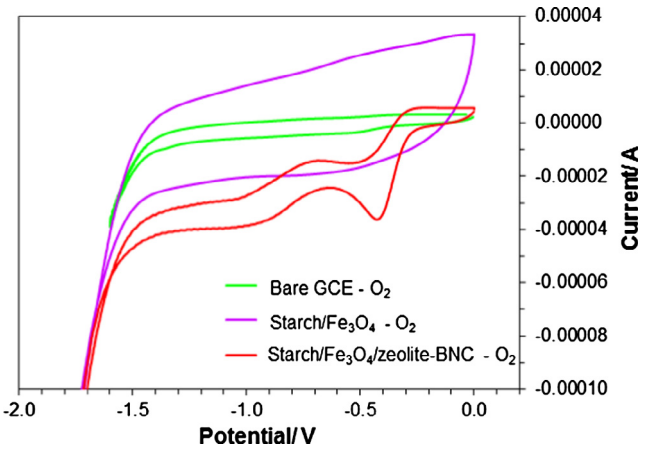


**Fig. 9** Cyclic voltammetry for bare GCE, starch/$Fe_3O_4$, starch/$Fe_3O_4$/zeolite-BNC in $O_2$-saturated 0.1 M KOH.

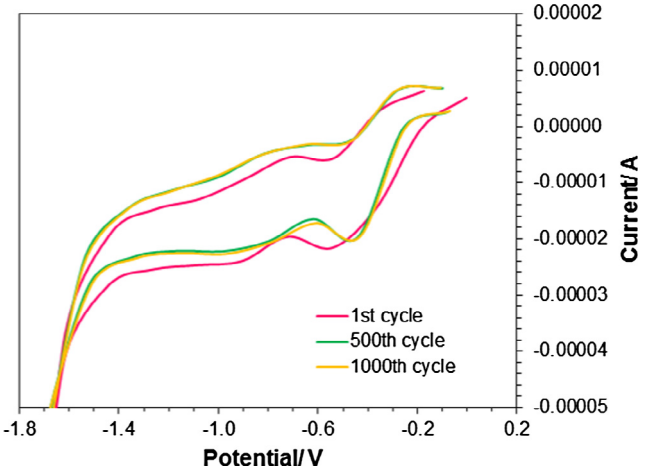


**Fig. 12** Cyclic voltammetry for starch/$Fe_3O_4$/zeolite-BNC after 1st, 500th and 1000th cycles.

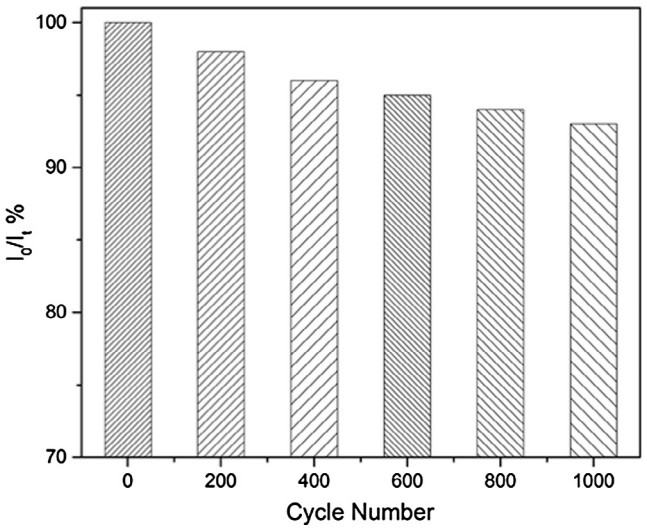


**Fig. 13** Plot of cycle number versus current after repeated cycles of BNC by cyclic voltammetry in $O_2$-saturated 0.1 M KOH.

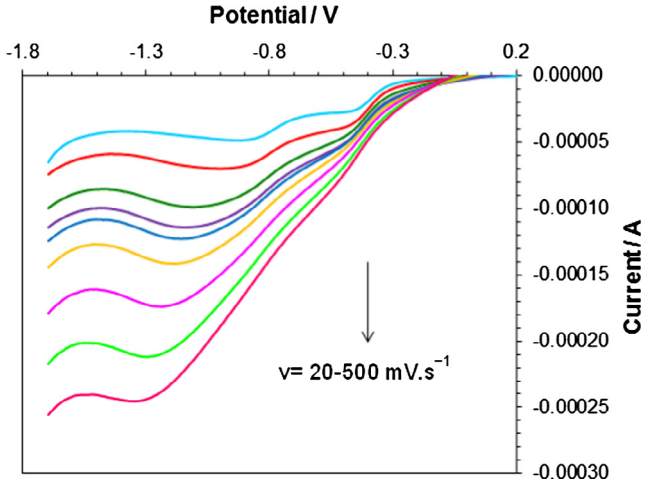


**Fig. 14** LSV of the BNC in $O_2$-saturated 0.1 M KOH at the scan rates of 20, 50, 100, 125, 150, 200, 300, 400 and 500 mV $s^{-1}$.

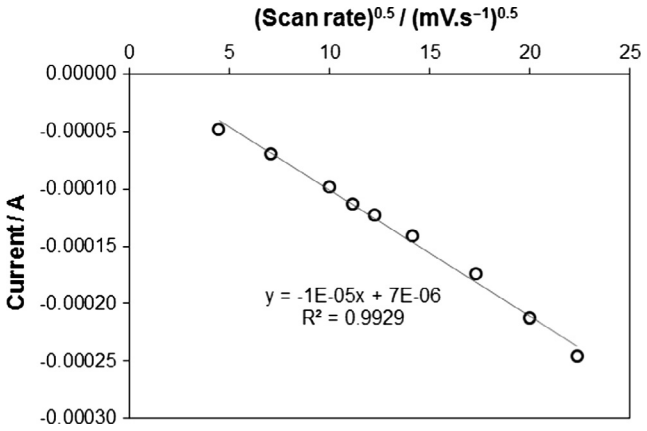


**Fig. 15** Plot showing square root of the scan rate versus current.

The performance of the BNC was further studied by LSV technique at different scan rates. As it can be seen in the Fig. 14, the peak current values of ORR decline by increasing the scan rate. The magnitudes of peak current change linearly with increasing the square root of scan rate (Fig. 15). The equation in the current versus $\upsilon^{0.5}$ graph indicated that the ORR is governed by the diffusion control process but the non-zero intercept shows that the ORR is not a fully controlled by diffusion manner. The second peak potentials shifted slightly to more negative values at higher scan rates which demonstrate the sluggish kinetics of intermediates that generated during the first reduction step on the BNC.

## 4. Conclusions

In conclusion, the green synthesis of starch/$Fe_3O_4$/zeolite–BNC was successfully developed without utilizing any toxic chemical and solvent. The UV–vis spectrum underwent transformation with the observation of plasmon resonance attributed to the formation of $Fe_3O_4$-NPs. PXRD analysis revealed high purity and crystallinity of starch/$Fe_3O_4$/zeolite–BNC. The highly distributed $Fe_3O_4$-NPs with an average diameter and standard deviation of 9.24 ± 3.57 nm were observed over the surface of zeolite. The formation of starch stabilized $Fe_3O_4$-NPs on the surface of zeolite was verified by FESEM and EDX analysis. VSM analysis indicated the saturation magnetization and coercivity of BNC were 1.84 emu $g^{-1}$ and 17.76 G, respectively. The employed synthesis technique is an environmentally friendly, cost effective and facile method for the preparation of BNCs. As for the application in energy, the BNC was used in the ORR process with long stability after 1000 repeated cycles. The voltammograms show that the BNC is an applicable catalyst for reducing oxygen molecules which can be employed in oxygen involving reactions as a potential non-precious catalyst.

## Acknowledgements

This research was supported by the grant funded by the Malaysian Ministry of Higher Education (Reference grant number PY/2015/05182 under Tier 1 grant). We would like to thank the Research Management Centre (RMC) and Malaysia-Japan International Institute of Technology (MJIIT), Universiti Teknologi Malaysia (UTM) for providing an excellent research environment and facilities.

## References

Abdullah, N.H., Shameli, K., Abdullah, E.C., Abdullah, L.C., 2017a. A facile and green synthetic approach toward fabrication of starch-stabilized magnetite nanoparticles. Chinese Chem. Lett. https://doi.org/10.1016/j.cclet.2017.02.015.

Abdullah, N.H., Shameli, K., Etesami, M., Chan Abdullah, E., Abdullah, L.C., 2017b. Facile and green preparation of magnetite/zeolite nanocomposites for energy application in a single-step procedure. J. Alloys Compd. 719, 218–226. https://doi.org/10.1016/j.jallcom.2017.05.028.

Ahmad, M. Bin, Shameli, K., Yunus, W.M.Z.W., Ibrahim, N.A., Darroudi, M., 2010. Synthesis and characterization of Silver/Clay/Starch bionanocomposites by green method. Aust. J. Basic Appl. Sci. 4, 2158–2165.

Basavegowda, N., Magar, K.B.S., Mishra, K., Lee, Y.R., 2014. Green fabrication of ferromagnetic $Fe_3O_4$ nanoparticles and their novel catalytic applications for the synthesis of biologically interesting benzoxazinone and benzthioxazinone derivatives. New J. Chem. 38, 5415–5420.

Belibi, P.C., Daou, T.J., Ndjaka, J.M.B., Michelin, L., Brendlé, J., Nsomd, B., Durand, B., 2013. Tensile and water barrier properties of cassava starch composite films reinforced by synthetic zeolite and beidellite. J. Food Eng. 115, 339–346. https://doi.org/10.1016/j.jfoodeng.2012.10.027.

Bukowska, A., Bukowski, W., Hus, K., Depciuch, J., Parlińska-Wojtan, M., 2017. Synthesis and Characterization of New functionalized polymer-$Fe_3O_4$ nanocomposite particles. Express Polym. Lett. 11, 2–13465. https://doi.org/10.7569/JRM.2013.634119.

Chang, P.R., Zheng, P., Liu, B., Anderson, D.P., Yu, J., Ma, X., 2011. Characterization of magnetic soluble starch-functionalized carbon nanotubes and its application for the adsorption of the dyes. J. Hazard. Mater. 186, 2144–2150. https://doi.org/10.1016/j.jhazmat.2010.12.119.

Chen, C., Byles, C.F.H., Buffet, J.-C., Rees, N.H., Wu, Y., O'Hare, D., 2016. Core–shell zeolite@aqueous miscible organic-layered double hydroxides. Chem. Sci. 7, 1457–1461. https://doi.org/10.1039/C5SC03208C.

Chen, D., Tang, Q., Li, X., Zhou, X., Zang, J., Xue, W.Q., Xiang, J. Y., Guo, C.Q., 2012. Biocompatibility of magnetic Fe3O4 nanoparticles and their cytotoxic effect on MCF-7 cells. Int. J. Nanomed. 7, 4973–4982. https://doi.org/10.2147/IJN.S35140.

Cheng, K., Kou, Z., Zhang, J., Jiang, M., Wu, H., Hu, L., Yang, X., Pan, M., Mu, S., 2015. Ultrathin carbon layer stabilized metal catalysts towards oxygen reduction. J. Mater. Chem. A 3, 14007–14014. https://doi.org/10.1039/c5ta02386f.

Chin, S.F., Pang, S.C., Tan, C.H., 2011. Green synthesis of magnetite nanoparticles (via Thermal Decomposition Method) with controllable size and shape. J. Mater. Environ. Sci 2, 299–302.

Chu, M., Zhang, Y., Yang, L., Tan, Y., Deng, W., Ma, M., Su, X., Xie, Q., Yao, S., 2013. A compartment-less nonenzymatic glucose–air fuel cell with nitrogen-doped mesoporous carbons and Au nanowires as catalysts. Energy Environ. Sci. 6, 3600–3604. https://doi.org/10.1039/c3ee41904e.

Darder, M., Aranda, P., Ruiz-hitzky, E., 2007. Bionanocomposites : a new concept of ecological, bioinspired, and functional hybrid materials. Adv. Mater. 19, 1309–1319. https://doi.org/10.1002/adma.200602328.

Das, B., Mandal, M., Upadhyay, A., Chattopadhyay, P., Karak, N., 2013. Bio-based hyperbranched polyurethane/$Fe_3O_4$ nanocomposites: smart antibacterial biomaterials for biomedical devices and implants. Biomed. Mater. 8, 35003. https://doi.org/10.1088/1748-6041/8/3/035003.

Delmondo, L., Salvador, G.P., Munoz-Tabares, J.A., Sacco, A., Garino, N., Castellino, M., Gerosa, M., Massaglia, G., Chiodoni, A., Quaglio, M., 2016. Nanostructured MnxOy for oxygen reduction reaction (ORR) catalysts. Appl. Surf. Sci. 388, 631–639. https://doi.org/10.1016/j.apsusc.2016.03.224.

Dung, T.T., Danh, T.M., Hoa, L.T.M., Chien, D.M., Duc, N.H., 2009. Structural and magnetic properties of starch-coated magnetite nanoparticles. J. Exp. Nanosci. 4, 259–267.

Freeman, D.C., Stamires, D.N., 1961. Electrical conductivity of synthetic crystalline zeolites. J. Chem. Phys. 35, 799–806. https://doi.org/10.1063/1.1701219.

Gautam, V., Srivastava, A., Singh, K.P., Yadav, V.L., 2015. Preparation and characterization of polyaniline, multiwall carbon nanotubes, and starch bionanocomposite material for potential bioanalytical applications. Polym. Compos. 1–11. https://doi.org/10.1002/pc.23608.

Ghazanfari, M.R., Kashefi, M., Shams, S.F., Jaafari, M.R., 2016. Perspective of $Fe_3O_4$ nanoparticles role in biomedical applications. Biochem. Res. Int., 32

Gnana kumar, G., Joseph Kirubaharan, C., Yoo, D.J., Kim, A.R., 2016. Graphene/poly(3,4-ethylenedioxythiophene)/Fe3O4 nanocomposite – an efficient oxygen reduction catalyst for the continuous electricity production from wastewater treatment microbial fuel cells. Int. J. Hydrogen Energy 41, 13208–13219. https://doi.org/10.1016/j.ijhydene.2016.05.099.

Gray, H.B., 2009. Powering the planet with solar fuel. Nat. Chem. 1, 7.

Hariani, P.L., Faizal, M., Ridwan, Marsi, Setiabudidaya, D., 2013. Synthesis and propeties of $Fe_3O_4$ Nanoparticles by Co-precipitation method to Removal Procion Dye. Int. J. Environ. Sci. Dev. 4, 336–340. https://doi.org/10.7763/IJESD.2013.V4.366.

Hui, C., Shen, C., Tian, J., Bao, L., Ding, H., Li, C., Tian, Y., Shi, X., Gao, H.-J., 2011. Core-shell $Fe_3O_4$@$SiO_2$ nanoparticles synthesized with well-dispersed hydrophilic $Fe_3O_4$ seeds. Nanoscale 3, 701–705. https://doi.org/10.1039/C0NR00497A.

Yang, Huijuan, Wang, Hui, Ji, Shan, Linkov, V., Wang, R., 2014. Synergy between isolated-$Fe_3O_4$ nanoparticles and CNx layers derived from lysine to improve the catalytic activity for oxygen reduction reaction. Int. J. Hydrogen Energy 39, 3739–3745.

Jane, J., 2006. Current understanding on starch granule structures. J. Appl. Glycosci. 53, 205–213.

Jiang, W.J., Gu, L., Li, L., Zhang, Y., Zhang, X., Zhang, L.J., Wang, J.Q., Hu, J.S., Wei, Z., Wan, L.J., 2016. Understanding the High Activity of Fe-N-C electrocatalysts in oxygen reduction: Fe/Fe3C nanoparticles boost the activity of Fe-Nx. J. Am. Chem. Soc. 138, 3570–3578. https://doi.org/10.1021/jacs.6b00757.

Kalantari, K., Ahmad, M. Bin, Shameli, K., Khandanlou, R., 2013. Synthesis of talc/$Fe_3O_4$ magnetic nanocomposites using chemical co-precipitation method. Int. J. Nanomed. 8, 1817–1823.

Kelemen, G., Schon, G., 1992. Ionic conductivity in dehydrated zeolites. J. Mater. Sci. 27, 6036–6040.

Kolen'ko, Y.V., Bañobre-López, M., Rodríguez-Abreu, C., Carbó-Argibay, E., Sailsman, A., Piñeiro-Redondo, Y., Cerqueira, M.F., Petrovykh, D.Y., Kovnir, K., Lebedev, O.I., Rivas, J., 2014. Large-scale synthesis of colloidal $Fe_3O_4$ nanoparticles exhibiting high heating efficiency in magnetic hyperthermia. J. Phys. Chem. C 118, 8691–8701. https://doi.org/10.1021/jp500816u.

Koriche, Y., Darder, M., Aranda, P., Semsari, S., Ruiz-Hitzky, E., 2014. Bionanocomposites based on layered silicates and cationic starch as eco-friendly adsorbents for hexavalent chromium removal. Dalt. Trans. 43, 10512–10520. https://doi.org/10.1039/c4dt00330f.

Liang, Y., Li, Y., Wang, H., Zhou, J., Wang, J., Regier, T., Dai, H., 2011. $Co_3O_4$ nanocrystals on graphene as a synergistic catalyst for oxygen reduction reaction. Nat. Mater. 10, 780–786. https://doi.org/10.1038/nmat3087.

Lin, L., Zhu, Q., Xu, A.W., 2014. Noble-metal-free Fe-N/C catalyst for highly efficient oxygen reduction reaction under both alkaline and acidic conditions. J. Am. Chem. Soc. 136, 11027–11033. https://doi.org/10.1021/ja504696r.

Liu, X.-W., Sun, T.-J., Hu, J.-L., Wang, S.-D., 2016. Composites of metal–organic frameworks and carbon-based materials: preparations, functionalities and applications. J. Mater. Chem. A 4, 3584–3616. https://doi.org/10.1039/C5TA09924B.

Loiola, A.R., Andrade, J.C.R.A., Sasaki, J.M., da Silva, L.R.D., 2012. Structural analysis of zeolite NaA synthesized by a cost-effective hydrothermal method using kaolin and its use as water softener. J. Colloid Interface Sci. 367, 34–39. https://doi.org/10.1016/j.jcis.2010.11.026.

Lu, W., Shen, Y., Xie, A., Zhang, W., 2010. Green synthesis and characterization of superparamagnetic $Fe_3O_4$ nanoparticles. J. Magn. Magn. Mater. 322, 1828–1833. https://doi.org/10.1016/j.jmmm.2009.12.035.

Ma, J., Zhu, W., Tian, Y., Wang, Z., 2016. Preparation of Zinc Oxide-starch nanocomposite and its application on coating. Nanoscale Res. Lett. 11, 200.

Please cite this article in press as: Abdullah, N.H. et al., Electrocatalytic activity of starch/$Fe_3O_4$/zeolite bionanocomposite for oxygen reduction reaction. Arabian Journal of Chemistry (2017), https://doi.org/10.1016/j.arabjc.2017.10.014

Ma, X., Changb, P.R., Yang, J., Yu, J., 2009. Preparation and properties of glycerol plasticized-pea starch/zinc oxide-starch bionanocomposites. Carbohydr. Polym. 75, 472–478.

Mao, G.-Y., Bu, F.-X., Wang, W., Jiang, D.-M., Zhao, Z.-J., Zhang, Q.-H., Jiang, J.-S., 2016. Synthesis and characterization of γ-$Fe_2O_3$/C nanocomposite as an efficient catalyst for the degradation of methylene blue. Desalin. Water Treat. 57, 9226–9236. https://doi.org/10.1080/19443994.2015.1027955.

Marija Grancaric, A., Tarbuk, A., Kovacek, I., Grancaric, A., 2009. Nanoparticles of activated natural zeolite on textiles for protection and theraphy. Chem. Ind. Chem. Eng. Q. 15, 203–210. https://doi.org/10.2298/CICEQ0904203G.

Mathur, A., Kushwaha, H.S., Vaish, R., Halder, A., 2016. Enhanced electrocatalytic performance of perovskite supported iron oxide nanoparticles for oxygen reduction reaction. RSC Adv. 6, 94826–94832. https://doi.org/10.1039/C6RA20002H.

Murbe, J., Rechtenbach, A., Topfer, J., 2008. Synthesis and physical characterization of magnetite nanoparticles for biomedical applications. Mater. Chem. Phys. 110, 426–433. https://doi.org/10.1016/j.matchemphys.2008.02.037.

Musyoka, N.M., Petrik, L.F., Hums, E., Kuhnt, A., Schwieger, W., 2015. Thermal stability studies of zeolites A and X synthesized from South African coal fly ash. Res. Chem. Intermed. 41, 575–582. https://doi.org/10.1007/s11164-013-1211-3.

Paixao, V., Monteiro, R., Andrade, M., Fernandes, A., Rocha, J., Carvalho, A.P., Martins, A., 2011. Desilication of MOR zeolite: conventional versus microwave assisted heating. Appl. Catal. A Gen. 402, 59–68. https://doi.org/10.1016/j.apcata.2011.05.025.

Park, K.S., Jin, S.-A., Lee, K.H., Lee, J., Song, I., Lee, B.-S., Kim, S., Sohn, J., Pak, C., Kim, G., Doo, S.-G., Kwon, K., 2016. Characterization of zeolitic imidazolate framework–derived polyhedral carbonaceous material and its application to electrocatalyst for oxygen reduction reaction. Int. J. Electrochem. Sci. 11, 9295–9306. https://doi.org/10.20964/2016.11.27.

Sadowska, K., Gora-Marek, K., Drozdek, M., Kustrowski, P., Datka, J., Martinez Triguero, J., Rey, F., 2013. Desilication of highly siliceous zeolite ZSM-5 with NaOH and NaOH/tetrabutylamine hydroxide. Microporous Mesoporous Mater. 168, 195–205. https://doi.org/10.1016/j.micromeso.2012.09.033.

Sagir, T., Huysal, M., Durmus, Z., Kurt, B.Z., Senel, M., Isık, S., 2016. Preparation and in vitro evaluation of 5-flourouracil loaded magnetite– zeolite nanocomposite (5-FU-MZNC) for cancer drug delivery applications. Biomed. Pharmacother. 77, 182–190.

Shameli, K., Ahmad, M. Bin, Zargar, M., Yunus, W.M.Z.W., Ibrahim, N.A., 2011. Fabrication of silver nanoparticles doped in the zeolite framework and antibacterial activity. Int. J. Nanomed. 6, 331–341. https://doi.org/10.2147/IJN.S16964.

Shchipunov, Y., 2012. Bionanocomposites: Green sustainable materials for the near future*. Pure Appl. Chem. 84, 2579–2607. https://doi.org/10.1351/PAC-CON-12-05-04.

Sun, M., Liu, H., Liu, Y., Qu, J., Li, J., 2015a. Graphene-based transition metal oxide nanocomposites for the oxygen reduction reaction. Nanoscale 7, 1250–1269. https://doi.org/10.1039/c4nr05838k.

Sun, M., Zhang, G., Liu, H., Liu, Y., Li, J., 2015b. α- and γ-Fe2O3 nanoparticle/nitrogen doped carbon nanotube catalysts for high-performance oxygen reduction reaction. Sci. China Mater. 58, 683–692. https://doi.org/10.1007/s40843-015-0082-x.

Sun, S., Miao, H., Xue, Y., Wang, Q., Li, S., Liu, Z., 2016. Oxygen reduction reaction catalysts of manganese oxide decorated by silver nanoparticles for aluminum-air batteries. Electrochim. Acta 214, 49–55. https://doi.org/10.1016/j.electacta.2016.07.127.

Sun, Y., Shen, Z., Xin, S., Ma, L., Xiao, C., Ding, S., Li, F., Gao, G., 2017. Ultrafine Co-doped ZnO nanoparticles on reduced graphene oxide as an efficient electrocatalyst for oxygen reduction reaction. Electrochim. Acta 224, 561–570. https://doi.org/10.1016/j.electacta.2016.12.021.

Tan, Y., Xu, C., Chen, G., Fang, X., Zheng, N., Xie, Q., 2012. Facile Synthesis of manganese-oxide-containing mesoporous nitrogen-doped carbon for efficient oxygen reduction. Adv. Funct. Mater 22, 4584–4591.

Tuo, Y., Liu, G., Dong, B., Zhou, J., Wang, A., Wang, J., Jin, R., Lv, H., Dou, Z., Huang, W., 2015. Microbial synthesis of Pd/$Fe_3O_4$, Au/$Fe_3O_4$ and PdAu/$Fe_3O_4$ nanocomposites for catalytic reduction of nitroaromatic compounds. Sci. Rep. 5, 13515. https://doi.org/10.1038/srep13515.

Udhoji, J.S., Bansiwal, A.K., Meshram, S.U., Rayalu, S.S., 2005. Improvement in optical brightness of fly ash based zeolite-A for use as detergent builder. J. Sci. Ind. Res. 64, 367–371.

Wang, D., Duan, H., Lü, J., Lü, C., Zheng, P., Shi, L., Dong, A., Jin, J., Ma, J., Zhao, D., 2017a. Fabrication of thermo-responsive polymer functionalized reduced graphene oxide@$Fe_3O_4$@Au magnetic nanocomposites for enhanced catalytic applications. J. Mater. Chem. A 5, 5088–5097. https://doi.org/10.1039/C6TA09772C.

Wang, L., Ji, H., Wang, S., Kong, L., Jiang, X., Yang, G., 2013a. Preparation of $Fe_3O_4$ with high specific surface area and improved capacitance as a supercapacitor. Nanoscale 5, 3793–3799. https://doi.org/10.1039/c3nr00256j.

Wang, L., Yang, H., Yang, J., Yang, Y., Wang, R., Li, S., Wang, H., Ji, S., 2016. The effect of the internal magnetism of ferromagnetic catalysts on their catalytic activity toward oxygen reduction reaction under an external magnetic field. Ionics (Kiel) 22, 2195–2202. https://doi.org/10.1007/s11581-016-1746-6.

Wang, R., Jia, J., Wang, H., Wang, Q., Ji, S., Tian, Z., 2013b. CNx - modified $Fe_3O_4$ as Pt nanoparticle support for the oxygen reduction reaction. J. Solid State Electrochem. 17, 1021–1028. https://doi.org/10.1007/s10008-012-1948-4.

Wang, S., Zhang, C., Chang, Q., 2017b. Synthesis of magnetic crosslinked starch-graft-poly(acrylamide)-co-sodium xanthate and its application in removing heavy metal ions. J. Exp. Nanosci. 1–15. https://doi.org/10.1080/17458080.2017.1321793.

Yan, Z., Lin, Z., Kai, M., Guozhu, M., 2014. The surface modification of zeolite 4A and its effect on the water-absorption capability of starch-g-poly (acrylic acid) composite. Clays Clay Miner. 62, 211–223.

Yu, J., Yang, J., Liu, B., Ma, X., 2009. Preparation and characterization of glycerol plasticized-pea starch/ZnO–carboxymethylcellulose sodium nanocomposites. Bioresour. Technol. 100, 2832–2841.

Zhang, M., Liu, X., Yan, Z., 2016. Soluble starch as in-situ template to synthesize ZSM-5 zeolite with intracrystal mesopores. Mater. Lett. https://doi.org/10.1016/j.matlet.2015.10.044.

Zhang, M., Pan, G., Zhao, D., He, G., 2011. XAFS study of starch-stabilized magnetite nanoparticles and surface speciation of arsenate Meiyi. Environ. Pollut. 159, 3509–3514.

Zhang, Y., Chu, M., Yang, L., Deng, W., Tan, Y., Ma, M., Xie, Q., 2014. Synthesis and oxygen reduction properties of three-dimensional sulfur-doped graphene networks. Chem. Commun. (Camb) 50, 6382–6385. https://doi.org/10.1039/c4cc01939c.